Supplement of Geosci. Model Dev., 16, 2095–2117, 2023
https://doi.org/10.5194/gmd-16-2095-2023-supplement

Geoscientific Model Development
Open Access
EGU

Supplement of

The emergence of the Gulf Stream and interior western boundary as key regions to constrain the future North Atlantic carbon uptake

Nadine Goris et al.

Correspondence to: Nadine Goris (nadine.goris@norceresearch.no)

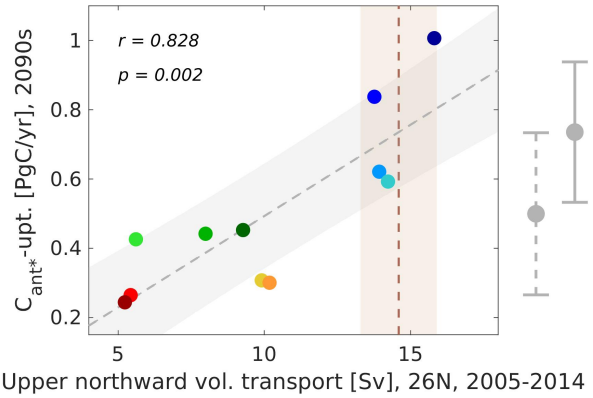

Figure S1. Emergent constraint between upper ocean northward volume transport accumulated between surface and 500 m depth for the years 2005-2014 (predictor) and the future North Atlantic C_{ant*} uptake (predictand) for the years 2090-2099 for our model ensemble. Shown are scatter-plot (color coding of models as in Fig. 1 of the main article), best fit linear regression (gray line) including the interval of the 68% projection uncertainty (gray shading), cross-correlation between simulated predictor and predictand as well as mean observational constraint and its uncertainty (dashed brown lines and light-brown shading). Associated estimates for the unconstrained model ensemble (dashed gray bar) and the emergent constraint (gray bar) are shown on the right side of the panels. See Appendix A of the main article for a detailed description of the considered observational estimate.

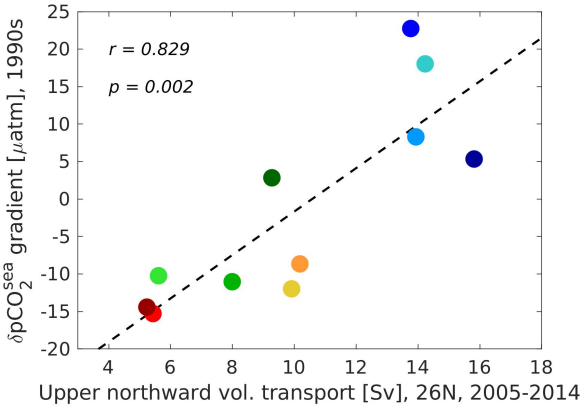

Figure S2. Relationship between (i) upper-ocean northward volume transport accumulated between surface and 500 m depth for the years 2005-2014 and (ii) the northward propagation of the winter pCO_2^{sea} anomaly for the years 1990-1999, here expressed as the difference between winter pCO_2^{sea}-anomalies for latitudes 26°-28°N and latitudes 40°-42°N. Shown are scatter-plot (color coding of models as in Fig. 1 of the main article), best fit linear regression (dashed black line) and cross-correlation between both quantities.

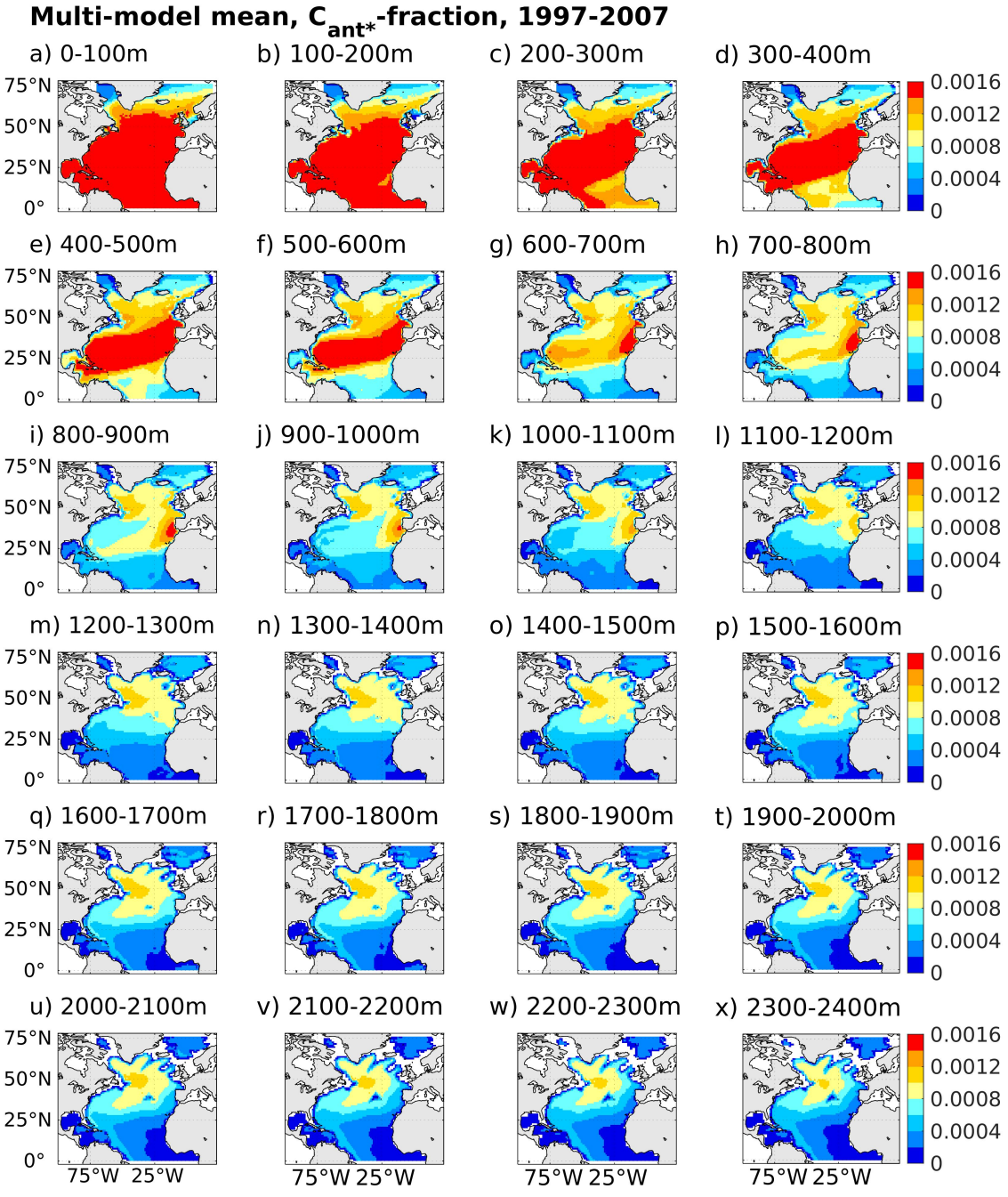

Figure S3. Contemporary fraction of the North Atlantic C_{ant*} multi-model mean for our considered model ensemble. Panels (a-x) displays results for different depth planes between surface and 2400m.

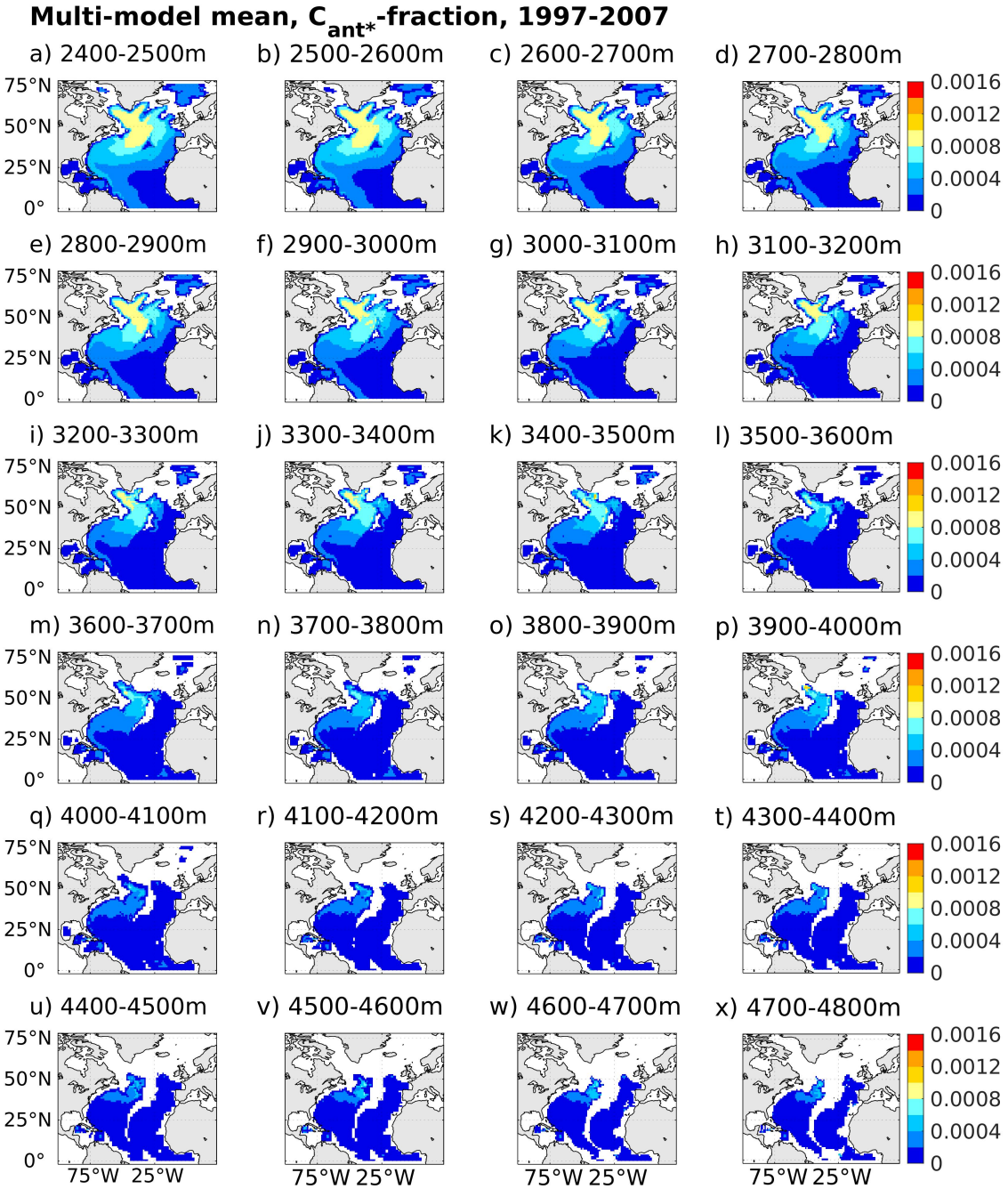

Figure S4. Contemporary fraction of the North Atlantic C_{ant*} multi-model mean for our considered model ensemble. Panels (a-x) displays results for different depth planes between 2400m and 4800m.

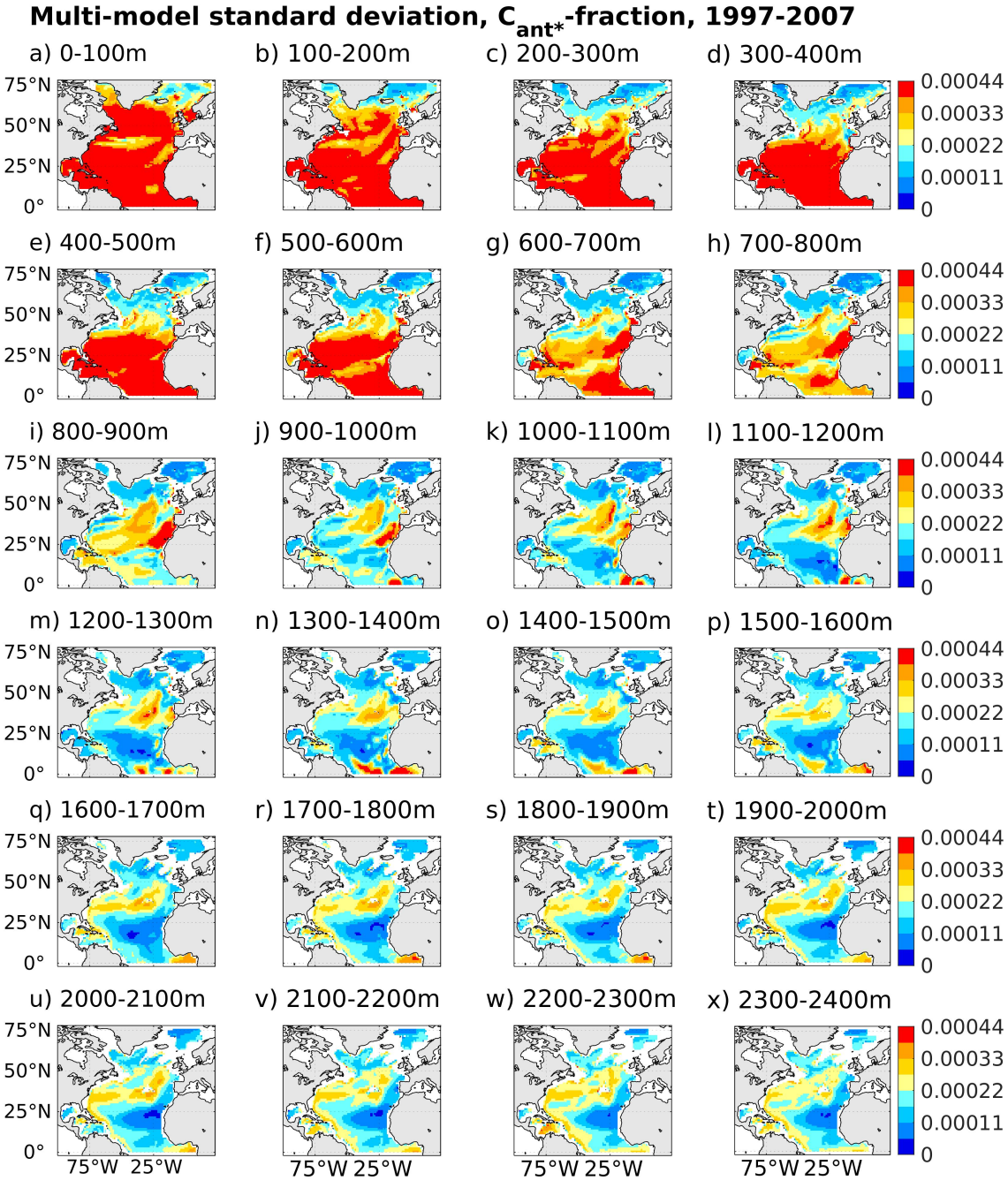

Figure S5. Contemporary fraction of the North Atlantic C_{ant*} multi-model standard deviation for our considered model ensemble. Panels (a-x) displays results for different depth planes between surface and 2400m. Non-eligible points are colored in different shades of blue.

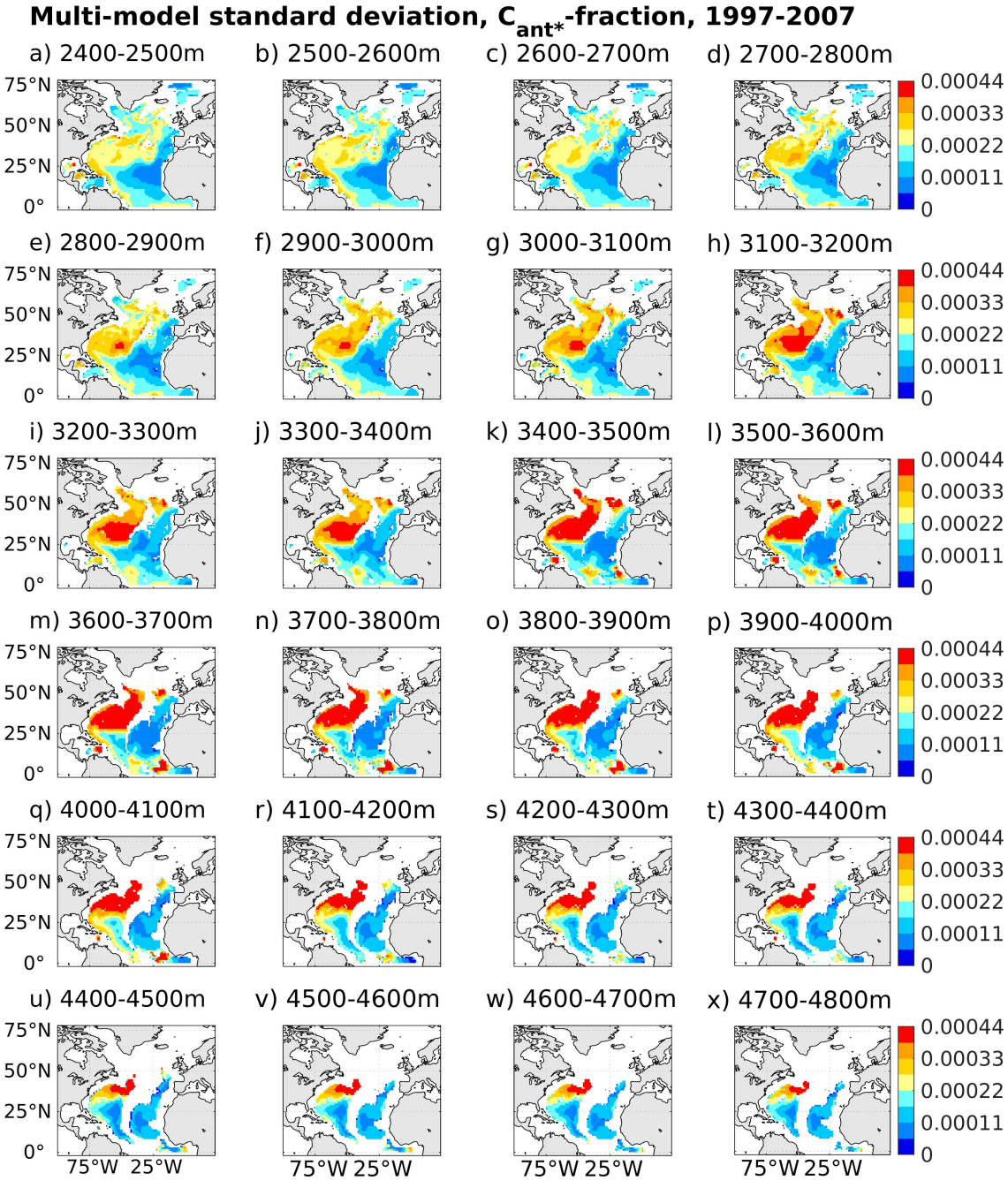

Figure S6. Contemporary fraction of the North Atlantic C_{ant*} multi-model standard deviation for our considered model ensemble. Panels (a-x) displays results for different depth planes between 2400m and 4800m. Non-eligible points are colored in different shades of blue.

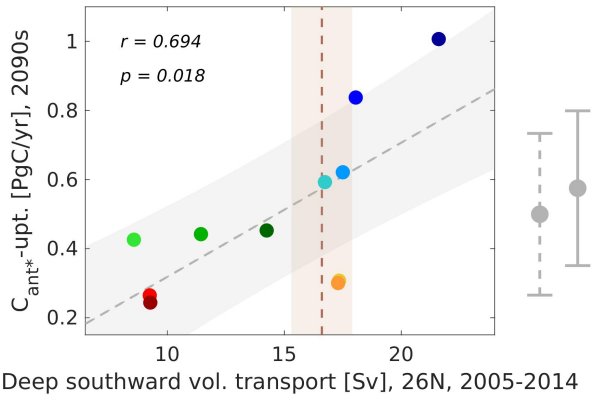

Figure S7. Emergent constraint between interior-ocean southward volume transport accumulated between 700 m and 4700 m depth for the years 2005-2014 (predictor) and the future North Atlantic C_{ant*} uptake (predictand) for the years 2090-2099 for our model ensemble. Shown are scatter-plot (color coding of models as in Fig. 1 of the main article), best fit linear regression (gray line) including the interval of the 68% projection uncertainty (gray shading), cross-correlation between simulated predictor and predictand as well as mean observational constraint and its uncertainty (dashed brown lines and light-brown shading). Associated estimates for the unconstrained model ensemble (dashed gray bar) and the emergent constraint (gray bar) are shown on the right side of the panels. See Appendix A of the main article for a detailed description of the considered observational estimate.